Aerospace Science and Technology 14 (2010) 295–301

Contents lists available at ScienceDirect

Aerospace Science and Technology

www.elsevier.com/locate/aescte

Numerical simulation of transverse side jet interaction with supersonic free stream

G. Aswin, Debasis Chakraborty *

Directorate of Computational Dynamics, Defence Research and Development Laboratory, P.O. Kanchanbagh, Hyderabad 58, India

ARTICLE INFO

Article history:
Received 27 May 2009
Received in revised form 18 January 2010
Accepted 4 February 2010
Available online 6 February 2010

Keywords:
Jet controlled aerospace Vehicle
CFD

ABSTRACT

The interference effects of side jets with supersonic cross flow for a lateral jet controlled missile are simulated numerically. Three-dimensional Navier–Stokes equations along with Menter's SST turbulence model are solved using a commercial CFD software. Effect of angle of attack, ratios of free stream and jet pressure, number of jets, etc. have been systematically studied. A very good agreement between computed and experimental surface pressure has been obtained. From detailed flow field analysis it is observed that the generation of pitching moment is taking place due to low pressure region behind the jet nozzle and the normal force and pitching moment is seen to vary linearly with the jet pressure ratio.

1. Introduction

The control demand for higher agility and enhanced maneuverability of a missile can be realized by side jet control. Although, the aerodynamic control surfaces work more efficiently in high densities and high velocities, the side jet control has quick response time compared to the aerodynamic control and is very effective in low stagnation pressure in the launch phase and low pressure at high altitude [1–3]. In its passive state, side jet control produces no additional drag as none of its components intrudes in the flow path. Thus lateral jet altitude control has been a preferred concept for missile systems.

The schematic of flow field caused by transverse jet exhausting into supersonic free stream is shown in Fig. 1. The interaction of the jet with the incoming boundary layer in the vehicle surface produce a complex flow structure consisting of a bow shock, separation region ahead of the jet, barrel shock and counter rotating vortex pair in the wake of the jet. These flow phenomena result in overpressure ahead of the side jet and the under pressure region downstream of the jet. By controlling this overpressure and under pressure regions by suitable location and operation of jets, the desired control forces can be achieved. The jet shape and its penetration into the supersonic free stream depend on various factors namely operating altitude, pressure ratios of the jet and free stream, diameter and shape of the side jet nozzle, free stream Mach number, etc. Champigny and Lacau [3] have presented various methods of investigations of side jet interaction with supersonic cross flow. With the advent of powerful computers and robust numerical algorithms, Computational Fluid Dynamics

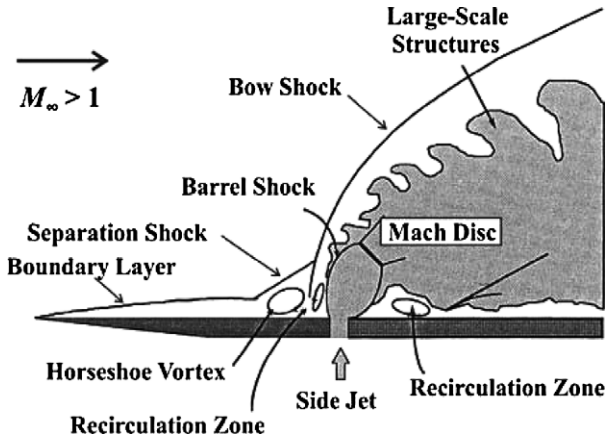

Fig. 1. Schematic of transverse jet injection flow field.

(CFD) can be used for direct solution of Jet Interaction (JI) flow field under many circumstances of application interest. Cassel [1] in his review of experimental and analytical modeling of jet interaction technology for aerospace vehicle control has described various aerodynamic interference problems and suggested a combination of CFD, wind tunnel and flight testing to understand the complex flow characteristics of jet interaction problem. Starting from two-dimensional solutions of Clark and Chan [5], CFD applications have matured to tackle practical missile geometry with angle of attack. Chamberlain [2] solved three-dimensional hypersonic jet interaction problem for a generic interceptor configuration at zero degree angle of attack using Navier–Stokes equations with Roe's scheme and analyzed detailed complex flow structure. Chan et al. [13,4] have performed CFD solution of complete jet in-

* Corresponding author. Tel.: +91 40 24583310; fax: +91 40 24340037.
E-mail address: debasis_cfd@drdl.drdo.in (D. Chakraborty).

1270-9638/$ – see front matter
doi:10.1016/j.ast.2010.02.001

Nomenclature

C_m	Moment coefficient
C_N	Normal force coefficient
C_p	Pressure coefficient
$(C_p)_{\text{diff}}$	Difference of pressure coefficient between jet and without jet
D	Diameter
F_s	Factor of safety
GCI	Grid Convergence Index
h_2, h_1	Grid sizes
M	Mach no., Moment about nose
N	Normal force
p	Pressure, order of accuracy in numerical scheme
q	Dynamic pressure
s	Reference area
α	Angle of attack
ϕ	Azimuthal angle
ε	Relative difference between two grids
γ	Ratio of specific heats

Subscripts

∞	Free stream condition
oj	Total condition of the jet
$o\infty$	Total free stream condition
with jet	With side jet on
without jet	Without side jet

teraction flow field for a slender missile at angle of attack, with a jet located forward on the missile and fins located on the afterbody. Srivastava [15] investigated numerically the effects of jet thrust, jet position and jet angle on the missile control through several case studies. Min et al. [10] developed a three-dimensional Navier–Stokes code and applied it to characterize the complex flow around lateral jet controlled missile. Roe's Flux difference splitting with Monotonic Upstream-Centered Scheme for Conservation Laws [MUSCL] [8] and Spalart Allmaras turbulence model [14] is used in the method. Aerodynamic analysis were performed to study the effect of jet Mach no., jet mass flow rate, circumferential jet position on the normal force and pitching moment coefficient of the missile. It is very clear that the interaction between supersonic free stream with side jet is very complex and systematic studies are required to find out the effect of various design parameters in getting an accurate estimate of aerodynamic forces of side jet controlled missile. By careful selection of the location of multiple jets and their pressure ratios, it is possible to determine an effective missile control and CFD techniques can play an important role in achieving this goal.

In this work, the experimental condition of Stahl et al. [16] is simulated numerically using a commercial software to understand the complex supersonic free stream and jet interaction problem for 1 jet, 2 jets, 3 jets positioned at different circumferential locations of an aerospace vehicle for various angle of incidence and pressure ratios. Detailed comparisons of experimental and computational surface pressure have been presented and various aerodynamic parameters are compared.

2. Description of the experimental condition for which the simulation is carried out

The experiments were conducted at DLR Trisonic wind tunnel at Cologne, Germany. The tunnel is of blow-down type with cross sectional area 600×600 mm^2 and permits test duration up to 60 sec. The configuration of tested model is presented in Fig. 2, which consists of a sharp cone, cylindrical fuselage and flare. The outer diameter (D) of cylindrical fuselage is 40 mm and its length is $3.2D$. The cone and flare of the model is of length $2.8D$ and $3D$ respectively. Three cylindrical jet nozzles of 4 mm diameter are positioned at $\phi = 180°$, 150° and 120° at a distance of $4.3D$ from the nose. Air as jet gas supplied to the individual jet nozzle from the reservoir has $M = 1$ at the exit. Different free stream Mach number (2.8 and 3.0), Reynolds number (0.5 and 1.9 million), jet pressure ratios (55, 110, 150, 200), angle of attack (−10°–15°) and different number of jets are considered in the experiment. Detailed pressure measurements are made at 4 generators corresponding to azimuthal angle of 180°, 150°, 120° and 90°. Schlieren picture and oil flow visualization has also been made to characterize the flow.

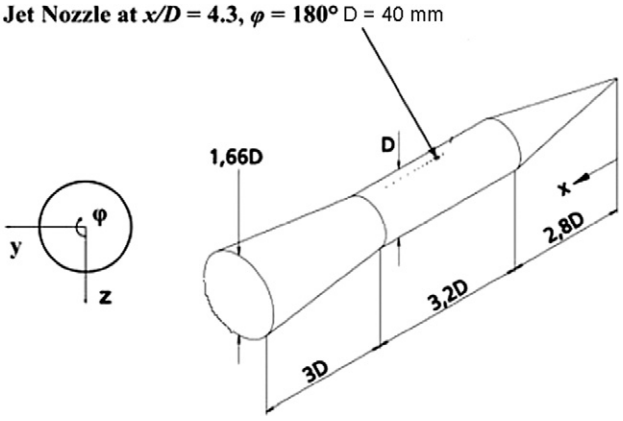

Fig. 2. Geometry of the tested model.

3. Computational methodology

Commercial CFD software CFX-10 [17] is used for the simulation. It solves 3-D Reynolds Averaged Navier–Stokes (RANS) equation based on finite volume approach on unstructured grid. The software has four major modules: a) *CFX Build* – imports Computer Aided Design (CAD) geometry or creates geometry and generates unstructured volume meshing based on the user input, b) *preprocessor* – sets up the boundary condition and initial field condition, c) *solver manager* – solves the flow field based on the grid and the boundary condition, and d) *postprocessor* – visualizes and extracts the results. Local time stepping has been used to obtain steady state solutions. In the present simulation, Menter's Shear Stress Transport (SST) turbulence model [9] is used.

4. Results and discussions

4.1. Computational grid

A hybrid grid consisting of extruded prism layers (6 layers fine grid with 0.1 mm spacing) near the wall and unstructured tetrahedron grid in the outer region is generated in the computational domain. Typical grid distribution in the computational domain is presented in Fig. 3. Grids are made very fine in the nose cone and the jet injection region to capture the complex flow features of the flow field. In the simulation, x-axis is taken along the longitudinal direction from the nose of the vehicle, while y- and z-axes are along the normal and lateral direction of the vehicle. As the free stream flow is supersonic, inflow domain is taken $1D$ ahead of the nose tip. The outflow boundary is placed at a distance of $20D$ from the missile base. The far field boundary at the jet injection

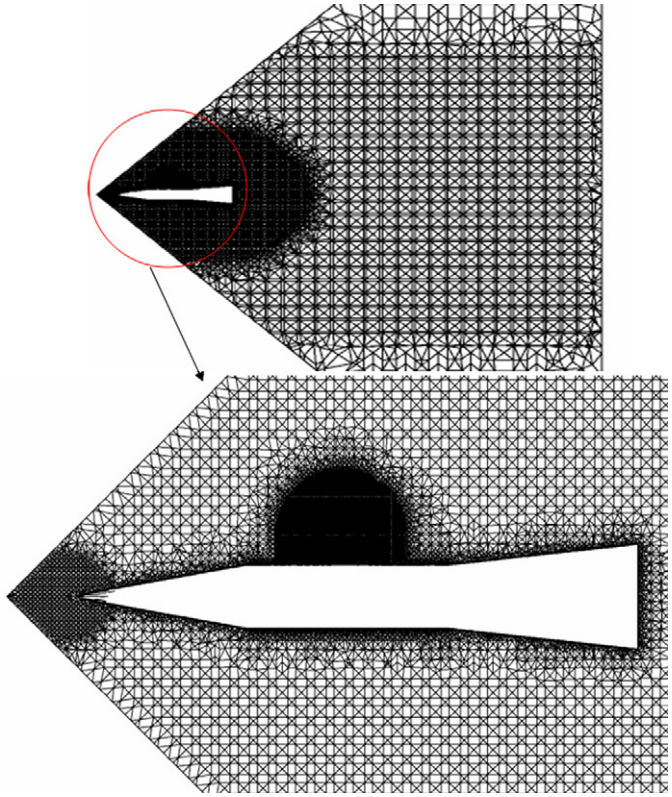

Fig. 3. Grid topology.

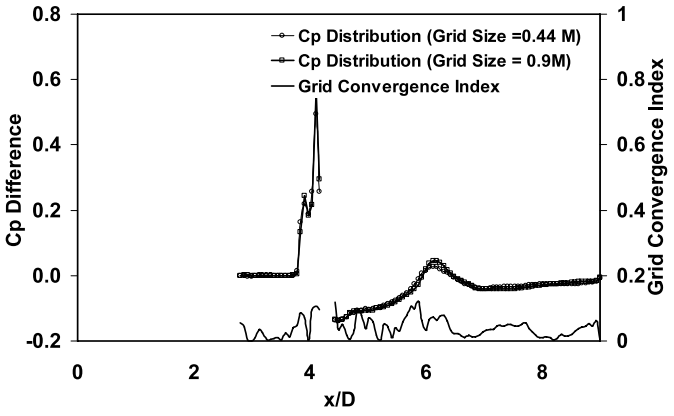

Fig. 4. Grid independence and grid convergence index.

zone is taken at a distance $5D$ from the model surface. Supersonic boundary conditions corresponding to free stream Mach number 3 is prescribed at the inflow plane and sonic condition is assumed at the injector exit plane. As the outflow boundary is supersonic, flow variables are extrapolated from the interior values.

Two different grids of size 0.44 and 0.9 millions are employed to find out the grid independence of the results. The surface pressure distribution for two different grids is compared for $P_{oj}/P_{\infty} = 55$ and $\alpha = 0^{\circ}$ in Fig. 4. A close match between the two is observed. An estimate of the error due to grid is also presented in the figure. For steady state boundary-value problem, the main source of numerical error in CFD is iterative convergence or grid convergence error [7]. Grid convergence or discretization error, which is the error of the solution of the difference equations compared to the exact solution of the partial differential equation, is the major source of numerical error. This error can be estimated by running the solution in two different grids (coarse and fine).

Table 1
Different cases of simulation.

Case no.	Angle of attack (deg)	Pressure ratios ($p_{oj}/p_{o\infty}$)	No. of jet
Case 1	0°	200	1
Case 2	−10°	200	1
Case 3	10°	200	1
Case 4	0°	150	1
Case 5	0°	110	1
Case 6	0°	55	1
Case 7	0°	150	2
Case 8	0°	150	3

The simplest of such estimate is given by the relative difference $\varepsilon = (f_2 - f_1)/f_1$ [6], where f represents any quantity of interest and the indices 1 and 2 refer to the fine and coarse grid solution respectively. (In the present calculation, surface pressure has been taken as the parameter of interest.) Roache [12] has proposed a grid-convergence index (GCI) as an error based on uncertainty estimate of the numerical solution as

$$\mathrm{GCI} = F_s \frac{1\varepsilon 1}{(h_2/h_1)^p - 1}$$

where h is the order of grid spacing, p is the order of accuracy of numerical scheme and F_s is a factor of safety. Roache [11] has suggested $F_s = 3$ for minimal of two grid calculations. For the present calculation p is equal 2 with h_2/h_1 equal to 2, GCI is order of ε. The axial distribution of the computed percentage error estimate based on pressure values between two grids are also presented in Fig. 4. Maximum error between two simulations is within 8%. This analysis indicates that the grid is adequate to capture most of features of the flow and the solution in grid independent.

4.2. Simulations with various flow parameters

A number of simulations are carried out to find out the effect of angle of attack, pressure ratio of jet and free stream, number of jets, etc., on the flow field of the lateral jet controlled missiles. The simulation Matrix is presented in Table 1. For all the cases, free stream Mach number and Reynolds number are 3.0 and 1.9 millions respectively. Simulations were also carried out without jet injection at various angles of attack to find out the effect of side jet on the overall forces and moments of on the missile.

The qualitative features of the flow field for $\alpha = 0^{\circ}$ and $p_{oj}/p_{o\infty} = 200$ (referred as baseline case) is presented in terms of Mach number distribution at the injection plane ($\phi = 180^{\circ}$) and in off injectional planes ($\phi = 150^{\circ}, 120^{\circ}, 90^{\circ}$) in Fig. 5. The attached shock at the nose, bow shock ahead of injection, separation region ahead of bow shock and separation shock are crisply captured in the simulation. The effect of injection is seen to slowly diminish as we move away from the injection plane. At $\phi = 90^{\circ}$, injection does not have any effect on the flow behavior. To analyze the spatial interference of the side jet with cross flow, axial distribution of computed pressure difference ($(C_p)_{\mathrm{diff}}$) between with and without the jet for the base line case at different azimuthal generators ($\phi = 180^{\circ}, 150^{\circ}$ and 90°) are compared with the experimental values in Figs. 6(a) and 6(b). $(C_p)_{\mathrm{diff}} = (C_p)_{\mathrm{with\ jet}} - (C_p)_{\mathrm{without\ jet}}$ defines the interference of the side jet with cross flow, where pressure coefficient C_p is defined as $C_p = 2(p - p_{\infty})/(\rho_{\infty}\gamma M_{\infty}^2)$. A very good match between the experimental and computational values is obtained. (The discontinuity in the graphs at $x/D = 4.3$ is due to the presence of the side jet.) Higher pressure is observed in front of the jet, while predominant low pressure zones are visible in the wake region. The area around the jet is dominated by high pressure zone. At $\phi = 90^{\circ}$, although the pressure rise is lower, the effect of high pressure in front of the jet is visible. The extent of low pressure zone in the wake is more for off injection plane.

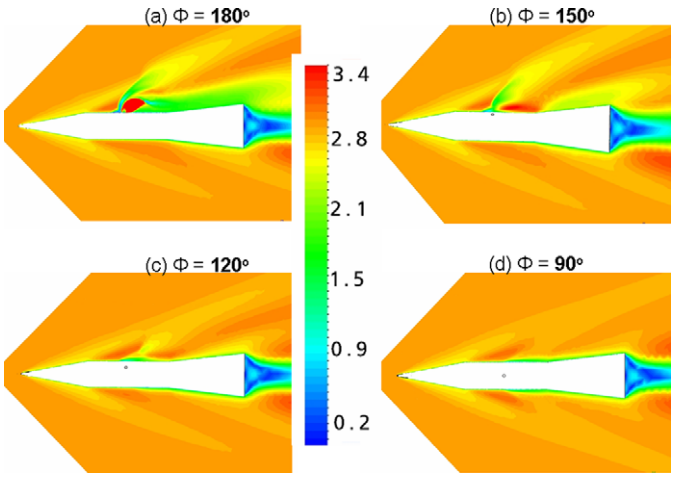

Fig. 5. Mach number contour at different azimuthal planes: (a) $\phi = 180°$, (b) $\phi = 150°$, (c) $\phi = 120°$, (d) $\phi = 90°$.

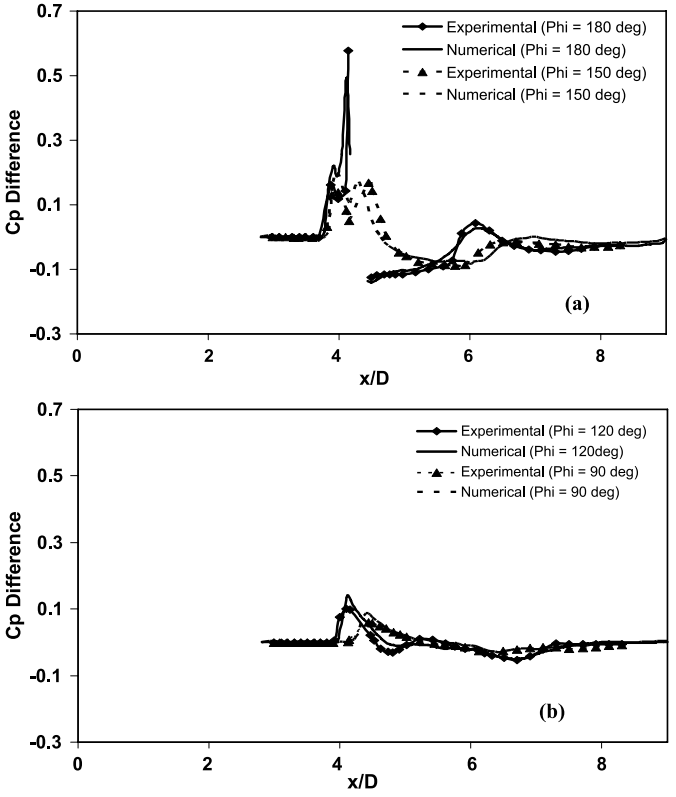

Fig. 6. Comparison of pressure distribution: (a) $\phi = 180°$ and $\phi = 150°$, (b) $\phi = 120°$ and $\phi = 90°$.

4.2.1. *Effect of angle of attack*

To find out the effect of angle of attack, simulations are carried for three different angle of attack ($\alpha = -10°, 0°$ and $+10°$) while keeping the pressure ratio constant (cases 2 and 3). The Mach number distribution at the injection plane at three angles of attacks $-10°$, $0°$ and $10°$ is shown in Fig. 7. For $\alpha = 0°$ and $-10°$, the shock from the nose tip is seen to interact with the bow shock caused by the injection. The separation region ahead of the injection is growing in size as α changes from $-10°$ to $+10°$. The computed pressure difference for different α at the plane of injection ($\phi = 180°$) is compared with the experimental result in Fig. 8. A reasonably good match is obtained. For $\alpha = 10°$, computations overpredict the surface pressure in the wake region. For $-10°$ angle of incidence, the predicted upstream separation is slightly downstream. The circumferential variation of surface pressure at $X/D = 4.3$ (injection location) for three different angle of attack is shown in Fig. 9. Circumferential variation is maximum for $\alpha = -10°$. Normal force coefficient C_N ($= N/qs$) and the moment coefficient $C_m = (M/qsD)$ (q, s, D are the dynamic pressure, reference area and missile diameter respectively) are plotted against angle of incidence in Figs. 10(a) and 10(b) respectively. Also the normal force and moment coefficient for without jet case are plotted in the figure. Moments are calculated about the nose of the

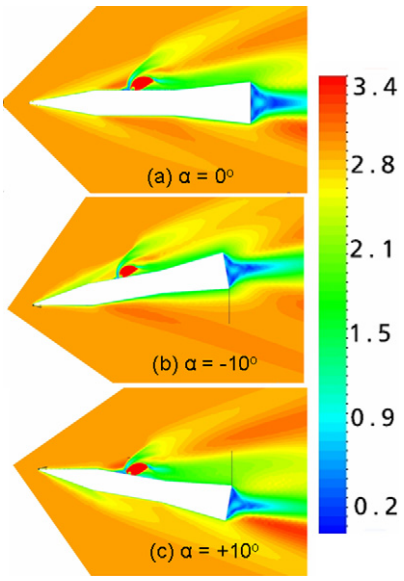

Fig. 7. Mach number contours at different angle of attacks: (a) $\alpha = 0°$, (b) $\alpha = -10°$, (c) $\alpha = +10°$.

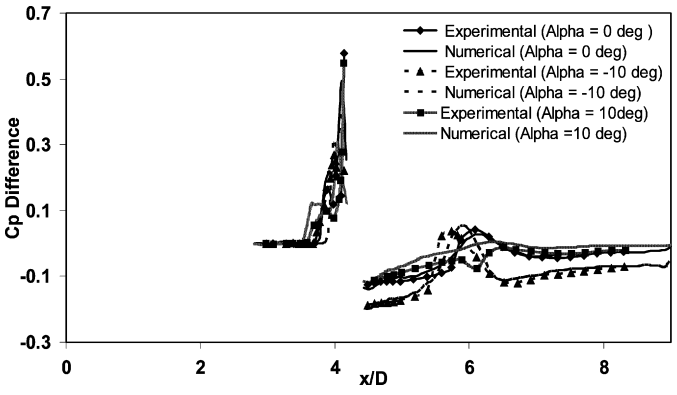

Fig. 8. Longitudinal pressure distribution comparison for different angles of attack.

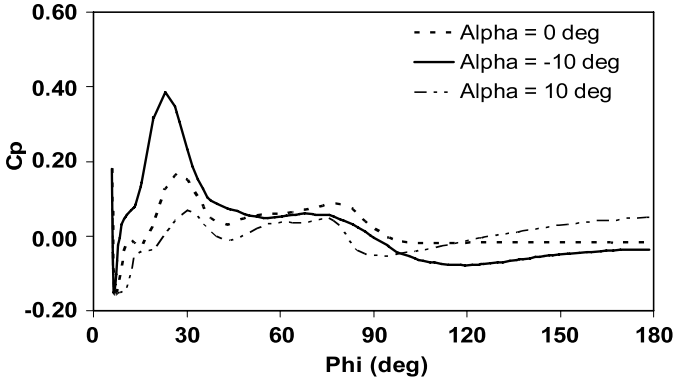

Fig. 9. Circumferential pressure distribution for different angles of attack.

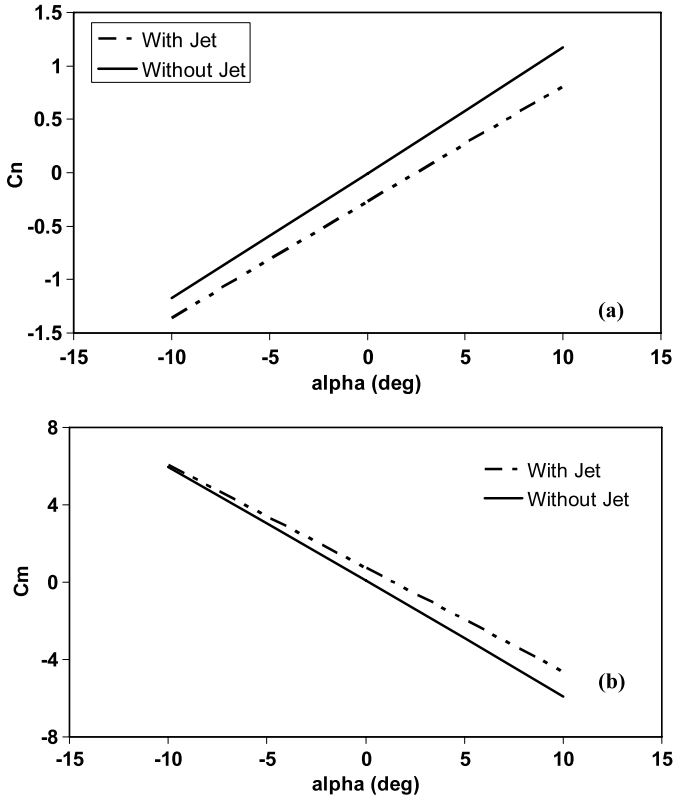

Fig. 10. Variation of (a) normal force coefficient and (b) moment coefficient with angle of attack.

vehicle. It is found that pitching moment characteristics of the missile are not greatly changed between with and without side jets for angle of attacks. So, angle of attack is not very effective for missile control by side jet, which is consistent with the observations made by Min et al. [10].

4.2.2. Effect of jet pressure variation

To investigate the effect of jet pressure on the flow characteristics of lateral jet controlled missiles, simulations are carried out for three other jet pressure ratios namely; $P_{oj}/P_\infty = 150$, 110 and 55 (cases 4, 5 and 6). The angle of incidence for these simulations is maintained at 0°. Mach number distribution in the vicinity of jet for the four pressures ratios $P_{oj}/P_\infty = 55$, 110, 150, 200 are shown in Fig. 11. With the increase in the pressure ratio, the size of the barrel shock increases but the inclination of the barrel shock varies a little. The bow shock in front of the nozzle moves upstream with the increase of the pressure ratio. The computed surface pressure distribution for $\phi = 180°$ generator is compared with measured values in Figs. 12(a) and 12(b) respectively. A very good match between the computed and measured surface pressure has been obtained for all the pressure ratios. Wall pressure increases considerably in the bow shock region for higher pressure. On the other hand, the low pressure region downstream of the injection point become significantly larger for the higher pressure ratios and the jet attaches itself to the missile surface. The low pressure regions behind the jet are the main contributor for increase in moment. The extended high pressure and low pressure zone in the missile surface for different pressure ratios are shown in the computed C_p contours in Fig. 13. The variation of normal force and moment coefficient with pressure ratios are presented in Table 2. Both the normal force and moments are seen to increase with the pressure ratios.

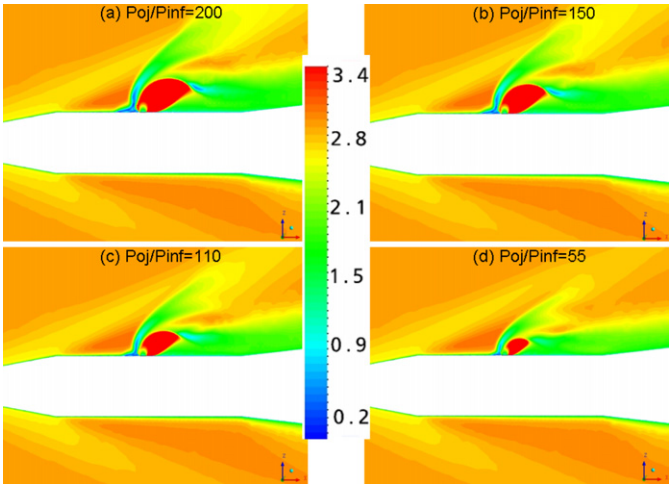

Fig. 11. Mach number contours for different jet pressure ratios: (a) $P_{oj}/P_\infty = 200$, (b) $P_{oj}/P_\infty = 150$, (c) $P_{oj}/P_\infty = 110$, (d) $P_{oj}/P_\infty = 55$.

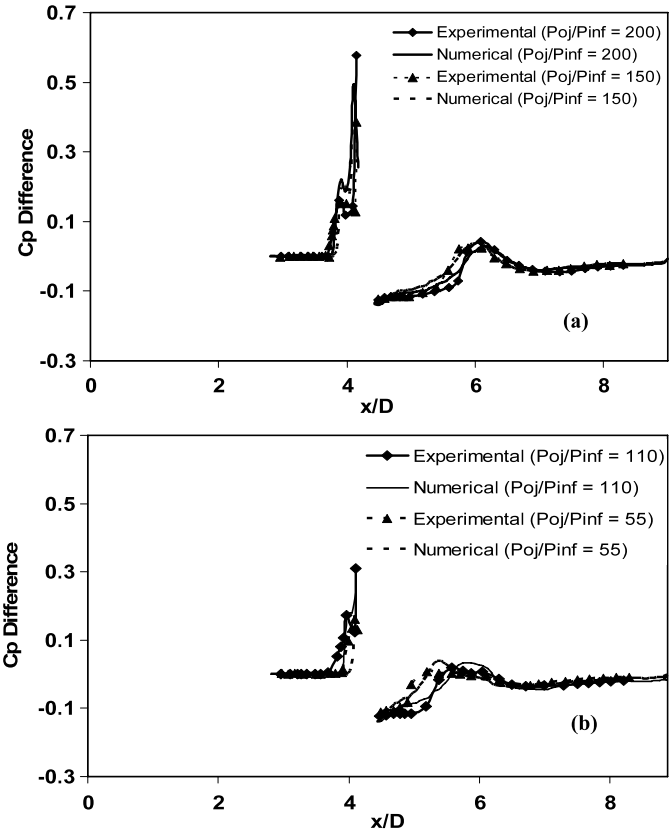

Fig. 12. Longitudinal pressure distribution for different pressure ratios: (a) $P_{oj}/P_\infty = 200$ & 150, (b) $P_{oj}/P_\infty = 110$ & 55.

Table 2
C_N and C_m variations with pressure ratio.

Pressure ratios ($p_{oj}/p_{o\infty}$)	C_N	C_m
200	−0.273	0.743
150	−0.188	0.423
110	−0.122	0.190
55	−0.043	0.019

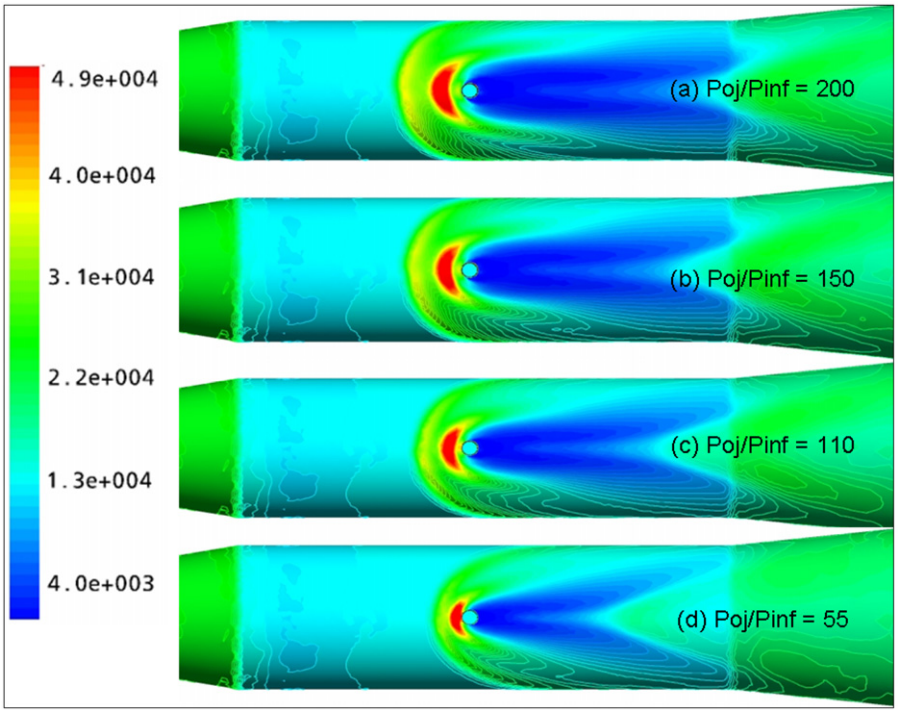

Fig. 13. Pressure contour for different jet pressure ratios: (a) $P_{oj}/P_\infty = 200$, (b) $P_{oj}/P_\infty = 150$, (c) $P_{oj}/P_\infty = 110$, (d) $P_{oj}/P_\infty = 55$.

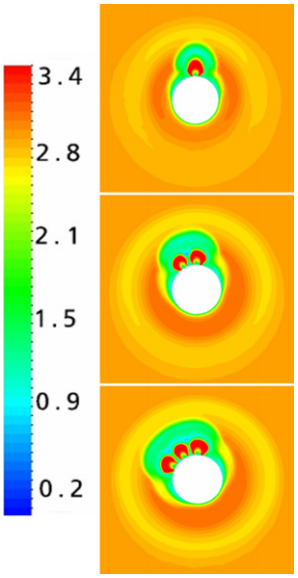

Fig. 14. Mach number contour for different number of jets circumferentially.

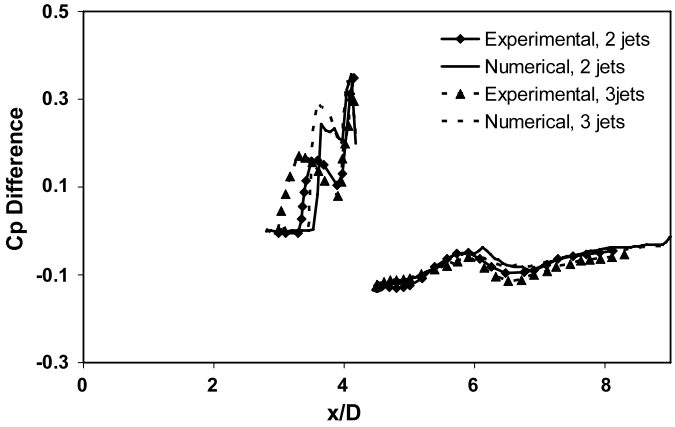

Fig. 15. Longitudinal pressure distribution for different number of jets circumferentially.

4.2.3. Effect of circumferential jet location

Simulations were carried out with multijet positioned at different circumferential location to find out the effect of jet position on the aerodynamic characteristics of the missile. Two different cases are simulated. In the first case, two jets are positioned at $\phi = 180°$ and 150° at $X/D = 4.3$ (case 7) and for the second case, three jets are positioned at $\phi = 180°$, 150° and 120° on same axial location (case 8). For the both the cases, free stream Mach number, angle of attack, Reynolds no. and pressure ratios are taken as 3.0, 0°, 1.9 millions and 150 respectively. The cross section view of computed Mach number distribution at $X/D = 4.3$ is compared between 1-jet, 2-jet and 3-jet cases in Fig. 14. It is clear from the figure, with the increase in the number of jet, the zone of interaction between the free stream and jets has increased. The computed surface pressures for 2-jet and 3-jet cases for $\phi = 180°$ are compared with the experimental value in Fig. 15. Although, a good match is obtained for the low pressure region behind the jets, the predicted separation ahead of the bow shock is in downstream location compared to the measured values. Mismatch of upstream separation location between the computation and experiment for 3-jet case is more compared to the 2-jet case. The computed normal force and moment coefficients 1 jet, 2 jets and 3 jets are compared in Table 3. Both C_N and C_m are seen to increase almost linearly with the increase of number of jets.

Table 3
C_N and C_m variations for multijet cases.

Cases	Mach no.	α	Reynolds no.	C_N	C_m
1 jet	3.0	0	1.9×10^6	−0.187	0.422
2 jets	3.0	0	1.9×10^6	−0.381	1.017
3 jets	3.0	0	1.9×10^6	−0.538	1.597

5. Conclusions

Numerical simulations are presented to study the interference effects of side jets for supersonic jet controlled missiles. Three-dimensional Navier–Stokes equations with Menter's SST turbulence model are solved in a hybrid grid using a commercial CFD software. The grid independence of the solution is demonstrated and an error estimate based on grid convergence index is presented. Parametric studies are carried out to find out the effect of angle of attack, jet pressure ratios and number of jets on the normal force and pitching moment coefficient. Very good comparison between experimental and computational surface pressures is obtained for different angles of attacks and jet pressure ratios which form the basis for further analysis. The predicted separation zone ahead of the bow shock is slightly upstream compared to the experimental values. It has been observed that angle of attack is not very effective for missile control by side jets. Pitching moments and normal force are seen to vary linearly with the jet pressure ratios and number of jets. Overpressure in the upstream position of jet and underpressure in the wake regions were mainly responsible for creating the moment of the vehicle. By careful selection of the location of multiple jets and their pressure ratios, it is possible to determine an effective missile control. Numerical simulations can play an important role in achieving this goal.

References

[1] L.A. Cassel, Applying jet interaction technology, Journal of Spacecraft and Rockets 40 (4) (2003) 523–537.
[2] R. Chamberlain, Calculation of three-dimensional jet interaction flow field, AIAA paper no. 90-2099.
[3] P. Champigny, R.G. Lacau, Lateral jet control for tactical missiles, AGARD Report 804, 1994, pp. 301–3057.
[4] S.C. Chan, R.P. Roger, G.L. Edwards, W.B. Brooks, Integrated Jet interaction CFD predictions and comparisons to force and moment measurement for a thruster altitude control missile, AIAA paper no. 93-3522.
[5] S.W. Clark, S.C. Chan, Numerical investigation of transverse jet for supersonic aerodynamic control, AIAA paper no. 92-0639.
[6] A.D. Cutler, P.M. Danehy, S.O'Byrne, C.G. Rodrigues, J.P. Drummond, Supersonic combustion experiment for CFD model development and validation, AIAA paper no. 2004-266.
[7] Guide for the verification and validation of computational fluid dynamic simulation, G-077-1998, AIAA, Reston, VA, 1998.
[8] C. Hirsch, Second Order Upwind and High Resolution Scheme in Numerical Computation of Internal and External Flow, vol. 2, John Wiley and Sons, 1988.
[9] F.R. Menter, Performance of popular turbulence models for attached and separated adverse pressure gradient flows, AIAA Journal 30 (8) (1992) 2066–2072.
[10] B. Min, J. Lee, Y. Byun, Numerical investigation of shock interaction effect on the lateral jet controlled missile, Aerospace Science and Technology 10 (2006) 385–393.
[11] P.J. Roache, Verification and Validation in Computational Science and Engineering, Hermon Publishers, New Mexico, 1998.
[12] P.J. Roache, Error base for CFD, AIAA paper no. 2003-0408.
[13] R.P. Roger, S.C. Chan, CFD study of the flow field due to supersonic jet exiting into a hypersonic stream from conical surface II, AIAA paper no. 93-2926.
[14] P.R. Spalart, S.R. Allmaras, A one-equation turbulence model for aerodynamic flows, La Recherche Aerospatiale 1 (1994) 5–21.
[15] B. Srivastava, Computational analysis and validation for lateral jet controlled missile, Journal of Spacecraft and Rockets 34 (5) (1997) 584–592.
[16] B. Stahl, H. Esch, A. Gulhan, Experimental investigation of side jet interaction with a supersonic cross flow, Aerospace Science and Technology 12 (2008) 269–275.
[17] User manual, CFX-10, Ansys, 2006.